Modeling internal tides and mixing over ocean ridges

Donald N. Slinn[1] and Murray D. Levine[2]

[1] Department of Civil and Coastal Engineering, University of Florida, Gainesville, Florida 32611-6590, 352-392-9537 x1431, slinn@coastal.ufl.edu

[2] College of Oceanic and Atmospheric Sciences, Oregon State University, Corvallis, Oregon, 97331-5503, 541-737-3074, mlevine@coas.oregonstate.edu

Abstract. Observations from the Hawaiian Ocean Mixing Experiment (HOME) Survey component suggest an increase in diapycnal mixing events during spring tides in a region above a steep slope. To study possible mixing mechanisms, we utilize numerical simulations of the benthic boundary layer, using a domain on the order of 200 m, with environmental parameters consistent with the conditions during HOME. In model results, when the barotropic tidal flow is upslope, the stratification near the boundary is greatly reduced as denser deep water is advected above the less dense water retained in the boundary layer. This leads to statically unstable situations and persistent strong mixing events that are several tens of meters thick and last for approximately one quarter of the tidal period. Conversely, during the down-slope tidal flow, denser fluid remains trapped in the boundary layer as less dense upslope fluid is advected downward, leading to very strong stratification near the boundary, that shuts down vertical mixing over the slope.

1. Introduction

The location, strength, and mechanisms that produce sufficient vertical mixing in the ocean to balance the large-scale thermo-haline circulation are not well understood but it is thought that internal tides play and important role (St. Laurent and Garrett, 2002). Significant resources have been dedicated to increase understanding of the role of tidally induced mixing in benthic boundary layers in the Hawaiian Ocean Mixing Experiment (HOME). HOME data show that nearly barotropic tides over steep ocean slopes can produce regions of shear instabilities that cause turbulent mixing. Our modeling studies are meant to assist in interpreting the field data and understanding the underlying dynamics. Boyd et al (2002) are investigating the energy pathway from barotropic tide to internal tide to enhanced diapycnal mixing in the HOME project. They deployed a mooring with vertical arrays of temperature and conductivity sensors and an upward looking ADCP for 2 months over the flank of a steep ridge (with a rise of 1.3 km in 10 km) in 1450 m of water about 50 km off Oahu (Boyd et al., 2002). The location of the measurements were ideally situated to capture interactions of the nearly barotropic tide with the sloping topography. The major axis of the barotropic tidal current is 10-20 cm/s and is aligned almost directly up-slope over a relatively smooth, two-dimensional section of the ridge.

Boundary layers over slopes have attracted significant attention as the probable location of strong diapycnal mixing responsible for elevating basin averaged vertical diffusivities. Armi (1978) suggested that the kinetic energy of the tides might provide a significant source of energy for strong boundary mixing, which then could be communicated to the ocean interior along isopycnals. This suggestion has been hotly debated in subsequent years, with others, (*e.g.*, Garrett, 1990; Eriksen, 1985) pointing to higher frequency internal waves, especially waves near critical frequency, as a more likely source of energy for boundary mixing. Interestingly, the ray of the internal tide is nearly critical around the mooring site, possibly permitting the testing of the different theories. Analysis of the field data has indicated that density inversions and regions of low Richardson number are often observed within 250 m of the slope.

Several simultaneous processes, driven by different dynamics, occur on the slope, and it is clear that a linear analysis is not sufficient to interpret the complexity of the physical interactions. For example, the barotropic tidal flow alone can raise isopycnals of order 200 m over a tidal cycle. At least five different important boundary features are expected to play significant roles over the slope in this case.

The first is the frictional turbulent boundary layer, with its characteristic, logarithmic, near-wall velocity profile. Due to the Coriolis force and frictional damping, and the time scales associated with the problem, it includes a benthic Ekman spiral (potentially including the slippery boundary layer mechanism described by MacCready and Rhines, 1991) that contains multiple inflection points and shear instabilities. The characteristic surface roughness, on a variety of horizontal length scales, can be an important factor in the thickness of the frictional boundary layer. Instabilities of related type have recently been modeled by Allen and Newberger (1998), associated with wind driven coastal upwelling, using a hydrostatic ocean model, with parameterizations (*i.e.*, Mellor-Yamada 2.5, [1982]) for boundary mixing, and shown to play an important role in cross shelf mixing. They have not yet, however, considered tidally driven boundary currents, nor have they looked into the benthic boundary layer itself, using a non-hydrostatic, eddy resolving model, such as we implement here to examine mixing dynamics in the boundary layer. This mechanism is the focus of the work reported here.

A second type of boundary layer feature that occurs on a slope is caused by the no-flux (no sources or sinks) boundary condition on the density (salinity) field. Phillips (1970) and Wunsch (1970) showed that isopycnals must intersect a sloping boundary perpendicular to the slope, and that this boundary condition produces a steady circulation across the slope with an upslope flow nearest to the boundary. The time scale to establish this flow is relatively fast compared to other processes in the problem, occurring on the order of a few buoyancy periods. Because the near boundary buoyancy driven circulation is additive with the mean tidal current during phases of upslope flow, and opposed to the tidal current during phases of down-slope tidal flow, it is possible that the interaction of the buoyancy driven currents and the tidally driven Ekman boundary layer could also cause asymmetries in phases in time series of local Richardson number and boundary mixing.

A third well known strong hydrodynamic instability associated with the oscillatory flow over the slope could also appear during phases of flow deceleration and flow reversal. In its simplest incarnation, this instability is associated with Stokes flow (1895) established in a boundary layer over an oscillating plate. In the oceanic context it occurs because the barotropic pressure gradient associated with the tide, and the buoyancy forces from displaced water masses near the slope cause the portion of the flow with least inertia, nearest the boundary, to change direction (say down-slope), while the flow above it is decelerating but still directed upslope. The vertical shear produced above the boundary contains a very strong inflectional instability (Blennerhassett and Bassom, 2002) and can be sufficient to overcome stratification and lead to pronounced shear induced K-H type mixing events during phases close to flow reversal.

The fourth important tidal benthic boundary phenomena is the near resonant forcing of internal tides over critically sloping topography. This inviscid process can focus or even trap baroclinic tidal energy near the boundary and lead to increased energy density and shear available to produce mixing. The near critical resonance process has been the focus of much of our past modeling work. [See Slinn and Riley, 1996, 1998a, 1998b (near critical frequency internal waves and currents on slopes); and Zikanov and Slinn, 2001 (along slope currents from obliquely incident internal waves).] Numerical experiments with a baroclinic tidal component can be forced with conditions matching the field experiments using the methods of Slinn and Riley, 1998a.

Finally, the fifth tidally induced flow feature suggested by the moored observations is the large-scale straining of the density field as the flow moves over finite topography. This occurs because the ocean ridge is a finite portion of the total water depth. As the barotropic tidal flow moves up the slope it must accelerate to conserve mass. During this acceleration phase the isopycnals will converge vertically, strengthening the density gradient. During the down-slope phase the opposite occurs and the background density gradient weakens. In the real ocean the degree to which this straining will occur depends on how much of the flow can go “around” three-dimensional topographic features, compared to how much must go “over” the ridge. Stratification encourages the flow to go “around”, while more of the flow goes “over” as the horizontal extent of the ridge increases. For input into our boundary layer model, there are at least four ways available to estimate the magnitude of the large-scale straining effect near the boundary layer. Each of these different boundary layer processes has its own characteristic time scales, associated with buoyancy, tidal period, Coriolis frequency, and turbulent diffusion and the interactions in the coupled problem are most nearly tractable using nonlinear models.

2. Modeling Approach

In our approach, we assume that the major dynamics of the system are represented in the Navier Stokes equations using the *f*-plane and Boussinesq approximations on a long, smooth slope. At relatively high Reynolds numbers, characteristic of the oceans, molecular diffusion is negligible and diffusivity is accomplished using turbulent eddy diffusivities with a turbulent Prandtl number (ν_τ / κ_τ) order 1. We write the non-

dimensionalized equations of motion for the large (resolved) scales of motion in a rotating and rotated (about the *y*-axis) reference frame. Here, α is the bottom slope; u and *x* are upslope; *v* and *y* are across or along the slope; and *w* and *z* are normal to the slope, such that gravity has a component in both the *x* and *z* directions, *i.e.*, $\vec{g} = -g\sin(\alpha)\hat{i} - g\cos(\alpha)\hat{k}$:

$$\frac{\partial u}{\partial t} + \vec{u}\cdot\nabla u + Ri\rho\sin\alpha = -\frac{\partial p}{\partial x} + \frac{\partial \tau_{1k}}{\partial x_k} + \frac{1}{Ro}v\cos\alpha, \qquad (1)$$

$$\frac{\partial v}{\partial t} + \vec{u}\cdot\nabla v = -\frac{\partial p}{\partial y} + \frac{\partial \tau_{2k}}{\partial x_k} - \frac{1}{Ro}\left[u\cos\alpha - w\sin\alpha\right], \qquad (2)$$

$$\frac{\partial w}{\partial t} + \vec{u}\cdot\nabla w + Ri\rho\cos\alpha = -\frac{\partial p}{\partial z} + \frac{\partial \tau_{3k}}{\partial x_k} - \frac{1}{Ro}v\sin\alpha, \qquad (3)$$

$$\frac{\partial \rho}{\partial t} + \vec{u}\cdot\nabla\rho = \frac{\partial \tau_{\rho k}}{\partial x_k} + w\cos\alpha + u\sin\alpha, \qquad (4)$$

$$\frac{\partial u}{\partial x} + \frac{\partial v}{\partial y} + \frac{\partial w}{\partial z} = 0. \qquad (5)$$

Here we have non-dimensionalized the velocity fields by the maximum tidally induced velocity, $U = U_M$ (= 20 cm/s), scaled time by U / L, scaled the lengths by the vertical domain size (*i.e.*, $L = L_z$ = 200 m), and the density field by the background density gradient. $Ro = U / f L$ is the Rossby number and $Ri = (N L / U)^2$ is the Richardson number. Using a constant value of ν_τ we examine $Re = U L / \nu_\tau$ between 30,000 and 120,000 and find little sensitivity on *Re* on the results. We also apply a spectral cut-off method of de-aliasing the calculations. We have further idealized the model by using a smooth plane sloping surface. The model is a derivative of that developed by Slinn and Riley (1998a), and employs third order variable time stepping, compact spatial differentiation, and the pressure projection method in a fractional time step approach, in which a Poisson equation for pressure is solved using Fast Fourier Transforms in the horizontal directions, and a compact 4th order direct solver in the vertical. We also use a stretched grid in the vertical direction, with increasing grid resolution near the ocean floor where shears are enhanced.

To this system we apply no heat flux and no-slip boundary conditions at the bottom slope, periodicity is assumed in the *x* and *y* directions and a free-slip condition is used at the upper boundary. An oscillatory barotropic body force representing the tidal forces is applied to the *x* momentum equation to induce the flow up and down the slope at the tidal frequency. The flow is made periodic in the upslope direction by subtracting off the constant background density gradient and solving the equations for the density perturbations. The buoyant effects of the background gradient appear in the terms that include the Richardson number and in the $w\cos\alpha + u\sin\alpha$ terms in the perturbation density equation. See Slinn and Riley (1998a) for details. By making the periodic

assumption, we acknowledge that we are focusing on mixing and boundary layer length scales (10's of meters), rather than attempting to model the full tidally induced flow throughout the water column on scales comparable to the overall topographic features (10's of kilometers) as is being pursued by other HOME investigators (*i.e.*, Holloway and Merrifield, 1999, Merrifield et al, 2001) with the Princeton Ocean Model (POM).

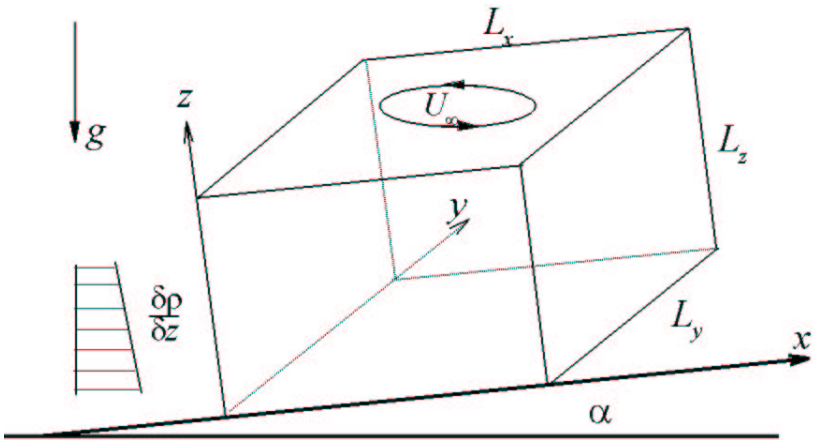

Figure 1. Schematic of model domain with physical dimensions L_x, L_y and L_z, a suggestion of the tidal ellipse of the free stream velocity (not to scale), the bottom slope α, and the background density gradient.

We are focusing on an idealized uniform slope, having horizontal dimensions much larger than the turbulent boundary layer thickness. Over a tidal cycle, flow external to the boundary layer may travel up and down the slope on the order of 3 kilometers (*e.g.*, with U_M ~ 20 cm/s and a half period of 6.2 hours). The slope itself at the HOME Survey Site extends fairly uniformly for approximately 15 km. We are modeling a domain with dimensions of 200 m on each side. In the simulations presented below the length scales are chosen to be $\tilde{L}_x = \tilde{L}_y = \tilde{L}_z = 200$ m (*i.e.*, non-dimensional lengths are $L_x = L_y = L_z = 1.0$). The typical turbulent boundary layer thickness we observe is on the order of 50 m, and the larger turbulent eddies in the domain are on the order of 20 m in diameter. In these simulations we used a grid resolution of 129 x 129 x 150 grid points (~2.5 million points). With the grid clustering near the boundary we resolve eddies down to approximately 1-2 m in diameter while smaller turbulent structures are modeled with the turbulent eddy viscosity model. These parameters are relatively ideal for the approximation of periodicity and suggest that conditions similar to those observed at this location on the slope should be representative of boundary layer flows occurring up and down and across the slope over a relatively wide region. A novel numerical (but physical) boundary condition is implemented at the upper boundary of the domain. Here the upper control surface is well below the free surface of the ocean, and we seek a boundary condition with minimal effect on the interior domain. For the velocity field we use a free-slip condition and on the density field we use a sponge layer that gradually relaxes back towards the mean density field of the idealized solution in the top 5% of the domain. The complexity comes from the fact that while the background density gradient

is constant in the flow external to the boundary layer; the value of the density field at the upper boundary changes significantly over the tidal cycle (*cf.* Figure 2).

Physical parameters used in the simulations are taken from the field measurements, *e.g.*, N = 2.2 x 10^{-3} s^{-1} (1.25 cph), the latitude is 21.8 N, giving a Coriolis parameter of 2.7 x 10^{-5} s^{-1}, and the tidal period of the M2 tide is 12.4 hours. With our non-dimensionalization, these yield a background Richardson number of 4.84 and a Rossby number of 37. We simulate the flow for 5-10 tidal cycles to develop a statistical average of mixing during different phases. The *x*-component of the free stream velocity induced by the barotropic tide is forced in the model to satisfy $U_\infty = U_M \cos(wt)$. No forcing is added to the *y* momentum equation, it is produced naturally through the Coriolis force.

3. Results

Results from the numerical simulations are presented, followed by an interpretation according to a simple model. Times series over two tidal periods ($2 < T < 4$) of the nondimensional density and up-slope velocity fields are shown in the boundary layer region ($z / L_z < 0.5$) in Figure 2. Increased internal wave activity and overturning of isopycnals are evident during phases of upslope flow. The signature of internal waves propagating away from the turbulent region are also evident, but decrease significantly during phases of down slope flow. The velocity fields show deviations from the free stream velocity out to heights of approximately 0.35. These are qualitatively similar to time series observed in the HOME field data for temperature and velocity fields (not shown).

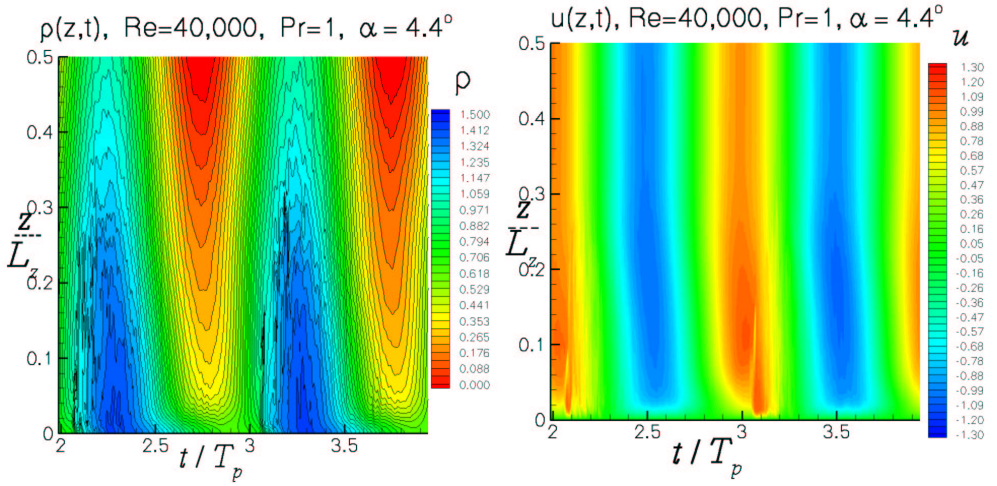

Figure 2. Nondimensional density and upslope velocity for tidal flow on a 4.4° slope.

Two-dimensional cross sections of the non-dimensional density field on the *x*-*z* plane located at $y_o = L_y/2$ during three different phases of the tide are shown in the left column of Figure 3. The second column of panels in Figure 3 presents the density field from an "end view" on an *y*-*z* plane located at $x_o = L_x/2$ at the same times. Together these

panels illustrate the most significant feature observed in the simulations: strong buoyant plumes rise from the boundary layer during a certain phase of the tidal cycle that lead to vigorous turbulent mixing in the benthic boundary layer for approximately 0.3 T. The third column of Figure 3 shows contours of the kinetic energy dissipation rate normalized by the kinematic viscosity and the buoyancy frequency squared ($\varepsilon / \nu N^2$) in the same *x*-*z* plane. The right-most column of Figure 3 also shows the dissipation rate from a "top-view" in an *x*-*y* plane parallel to the bottom boundary located at a height $z_o = 0.05\ L_z$. Higher values indicate the cores of eddies, the strong shear layer at the boundary, and other coherent vortical structures. The top row of panels is shown just after a time of maximum upslope flow (*i.e.*, t ≈ 1) as mixing begins to develop into turbulence and the two-dimensional buoyant plumes are released from the lighter fluid near the wall. The middle row of panels is shown during a phase of strong mixing, approaching the end of the phase of up-slope flow. The bottom row of panels is taken at a time of strong stratification, during a phase of down-slope flow when mixing has ceased.

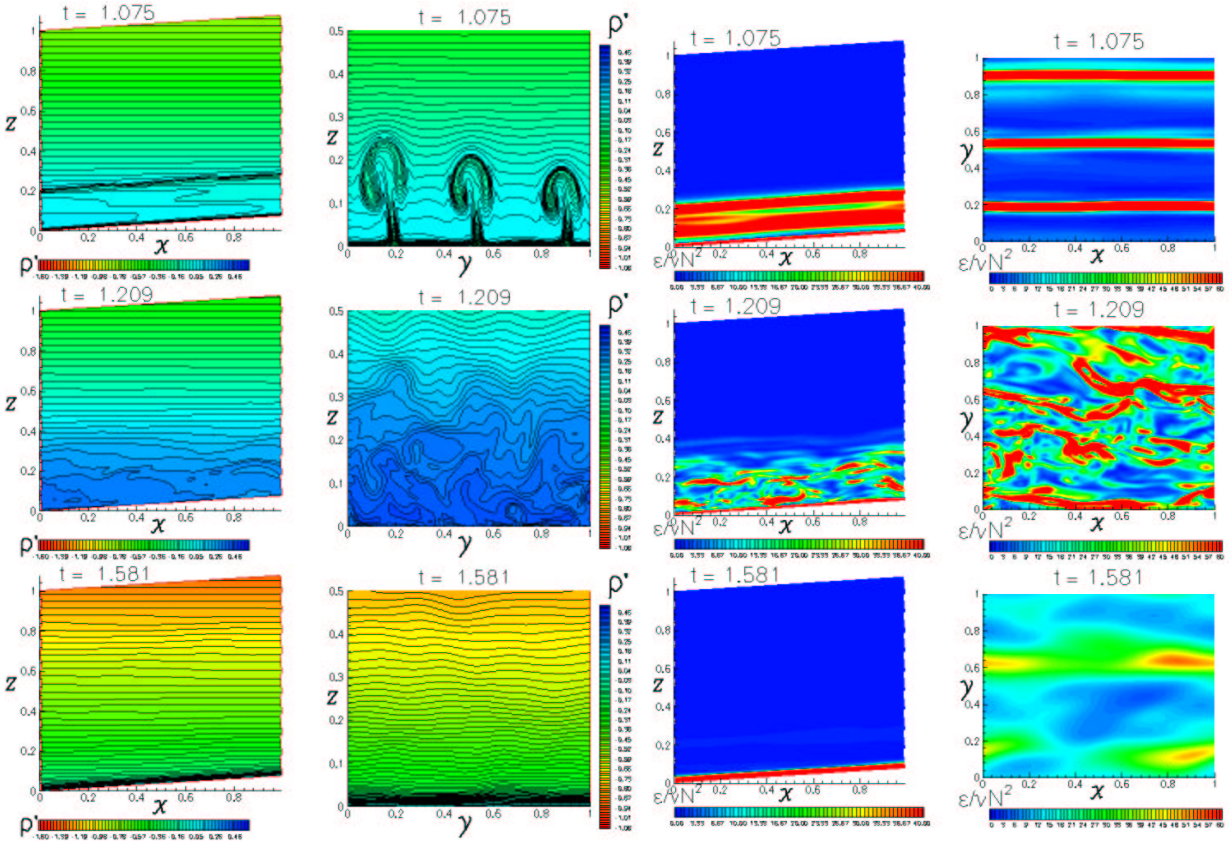

Figure 3. Density fields (left) and dissipation rate contours (right) during phases of flow instability (top row), turbulent mixing (middle row) and strong stratification (bottom).

Figure 4 shows projections of the velocity vectors in the same three planes as Figure 3. The top row is *x*-*z* (side view) planes, the center row is *x*-*y* (top view) planes, and the bottom row is *y*-*z* (end view) planes. Three-dimensional effects of stratified

turbulence are evident. Statically unstable situations are produced in regions within approximately 60 m ($z < 0.3$) of the boundary during phases of upslope flow.

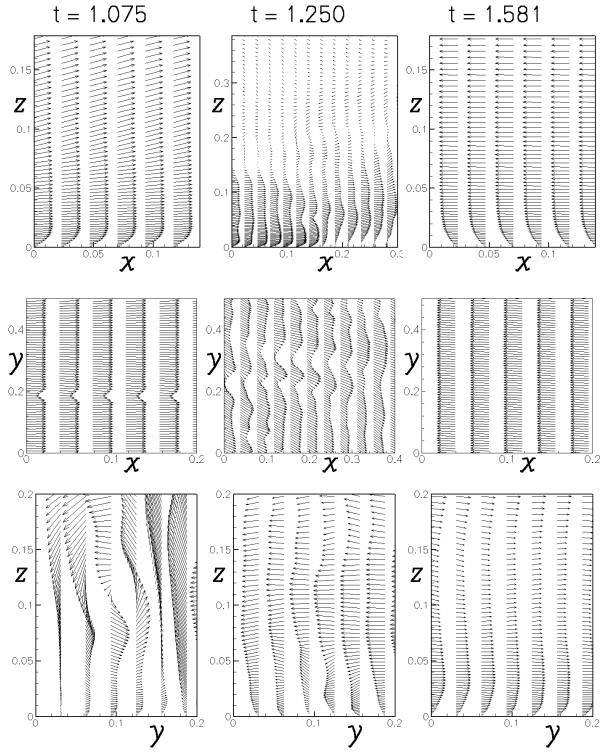

Figure 4. Velocity vectors during three phases of flow in three different 2D cross-sections. To enhance visibility three things are done: 1) the vectors in the center column are increased in length compared to the right and left columns when the flow is weak near flow reversal; 2) only one out of five columns of vectors are shown in the horizontal direction in each plane to increase spacing between vectors; 3) Each panel shows only a portion of the domain in that plane (i.e., the full x dimension extends to 1.0). Typically the boundary shear layer is resolved with 5-20 grid points.

The key physical process uncovered in the simulations is that there is a strong asymmetry during tidal phases caused by interactions between the boundary layer and the background stratification. An illustrative sketch is included in Figure 5. When the flow is upslope heavier fluid is moving up from below. The fluid previously located near the wall is lighter than the fluid coming to replace it, but the friction or turbulence near the wall prevents the lighter fluid from leaving as quickly as the new heavier fluid is approaching. This leads to a situation where the lighter, slower moving fluid is retained beneath the denser water external to the boundary layer. This unstable density structure greatly enhances turbulence production near the wall. The turbulence in turn produces a thicker boundary layer of slower moving intermediate density mixed fluid. The upslope flow persists for approximately 6 hours and turbulence is particularly evident for the latter 3 hours when the flow is decelerating. Decelerating flows are known to be more hydrodynamically unstable than steady or accelerating flows (Gad-El-Hak et al, 1984) but the effects observed here are thought to occur primarily during this phase (for this bottom slope) because it takes the first 3 hours of upslope flow to overcome the very

strong stratification that was produced near the boundary during the previous phase of down slope flow. The buoyancy period, external to the boundary layer, is approximately 0.8 hours, and hence, the stratified turbulence responds in a relatively short time scale compared to the duration of the flow conditions, and yet far from an instantaneous adjustment, as might be anticipated for buoyant fluid with a larger density difference. Soon after the onset of mixing the intermediate density mixed water produced in the boundary layer is also comparatively light to the deeper water still flowing upslope. The process repeats over and over during phases of upslope flow causing a quasi-steady turbulent layer with weak or unstable stratification near the boundary. We observe continuous production and release of buoyant plumes of water from the boundary layer for approximately 3 hours, during each cycle of upslope flow for these conditions. The turbulent layer becomes on the order of 50 - 80 m thick in these simulations.

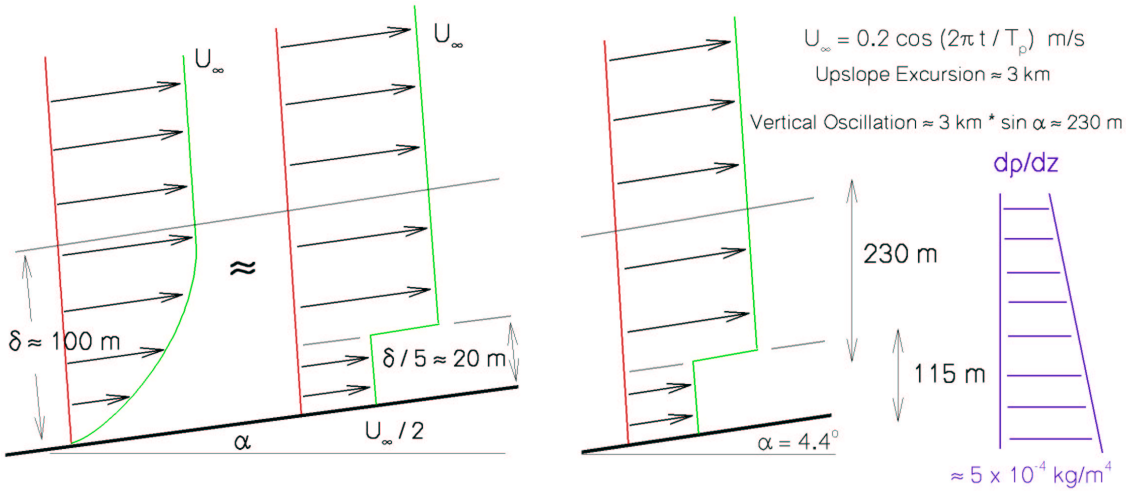

Figure 5. Illustrative sketch of boundary layer production of buoyancy flux. Left panel shows a typical boundary layer profile that could be idealized as a thinner layer of fluid moving at about half the velocity of the free stream. For the tidal flow used here with an upslope excursion of 3 km, therefore the free stream would move vertically 230 m, while the slower moving layer would only transverse 115 m. This would allow a layer of lighter fluid to move 115 meters above the heavier bottom retarded fluid in the boundary layer.

As the flow reverses downslope, other dynamical processes become more important and the near boundary fluid containing less inertia responds to the barotropic pressure gradient first and moves down-slope while the flow exterior to the boundary layer is still directed upslope. This final phase of the mixing cycle leads to the strongest (shear induced) turbulence close to the boundary. But the turbulent layer soon collapses, because frictional forces in the boundary layer during the down-slope phase of flow has the opposite effect from the upslope phase. Now buoyancy forces act to inhibit turbulent production as lighter stratified fluid from above is moved above the denser, slower moving boundary layer water that is retarded by friction near the wall. This eventually leads to much stronger stratification (by a factor of 2 to 10) across the boundary layer

than in the quiescent fluid. This stable situation is sufficient to inhibit turbulent production near the wall and reorganize the boundary layer into a parallel shear flow. Mixing ceases and remains negligible for approximately 6-8 hours until the flow again returns upslope. It takes approximately 2 hours of upslope flow, for the specified physical parameters (U_M, N, f, α) before the turbulence recommences in earnest. Similar behavior is suggested by the field data from HOME and a related asymmetry between induced mixing on flood and ebb tides in estuaries is well documented (*e.g.*, Simpson et al., 1990; van Aken, 1986, Chant and Stoner, 2001).

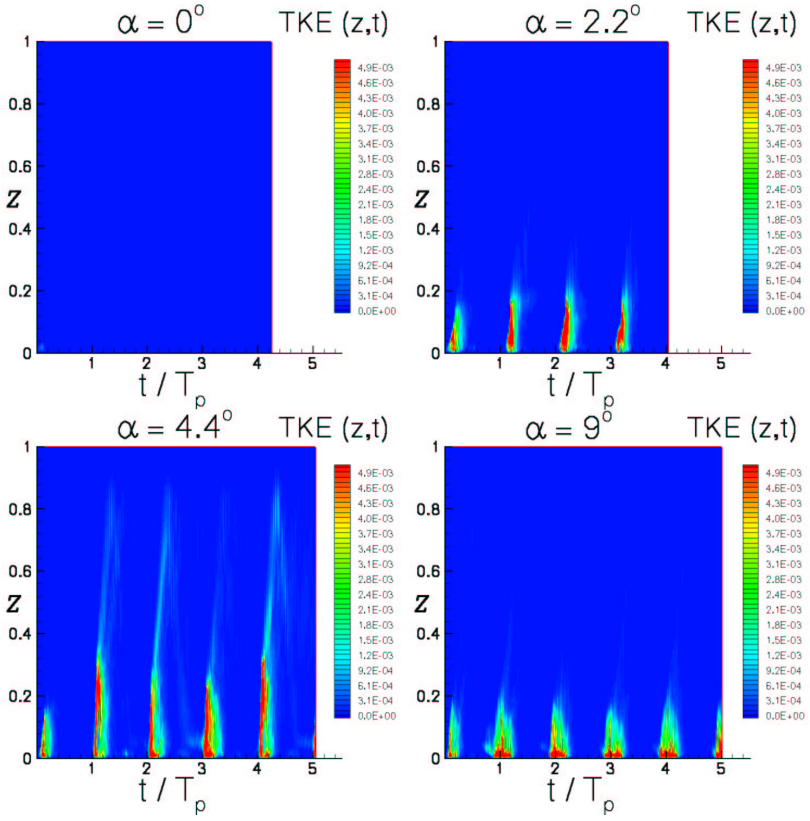

Figure 6. Horizontally averaged turbulent kinetic energy as a function of time and distance from the boundary for different bottom slopes.

We repeated the simulations in Case 1 with different values of the bottom slope, Reynolds number, and Prandtl number. Results of the horizontally averaged (in planes parallel to the boundary) turbulent kinetic energy as a function of time for different slopes are shown in Figure 6. The distance from the boundary that the turbulence reached was less for the other slopes. For the 9^o slope, the mixing begins earlier in the cycle and persists for longer duration but the plumes do not extend as far from the boundary. This is consistent with the interpretation (below) that there is greater buoyancy flux in this case and it is released sooner because the vertical distance traversed by the free stream velocity is twice as large as for the 4.4^o case. No turbulence is produced in the flat bottom case ($\alpha = 0$), indicating that the release of tidal potential energy, rather than interactions caused by the tidal kinetic energy alone are responsible for the mixing.

We utilize the time-averaged potential energy dissipation rate, χ, and flux Richardson number, $R_f = \chi / (\chi + \varepsilon)$, (mixing efficiency) to estimate the effects of the turbulent flow for different parameters, Pr, α, Re, etc. Results are shown in Figure 7.

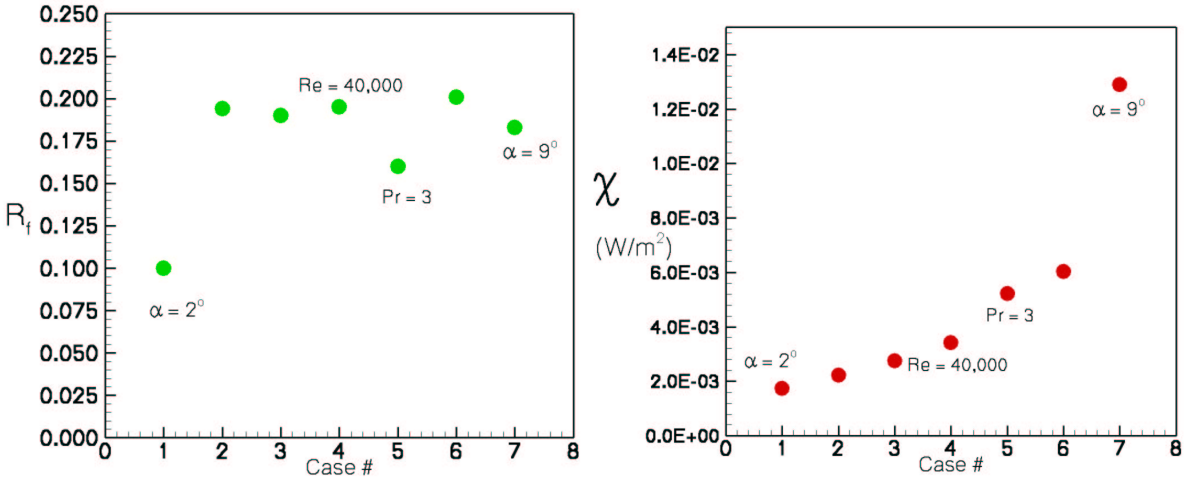

Figure 7. The mixing efficiency, R_f , and time averaged potential energy dissipation rate for numerical simulations with different Re, Pr, and bottom slope. Typically the mixing efficiency of the turbulence is close to 0.2.

With the simulations we also explore how the interior stratified fluid is exchanged with the boundary mixed regions. These aspects are investigated using numerical dye release and Lagrangian drifter experiments to indicate the horizontal exchange flows, typically seen along isopycnals and with components at the tidal and inertial periods.

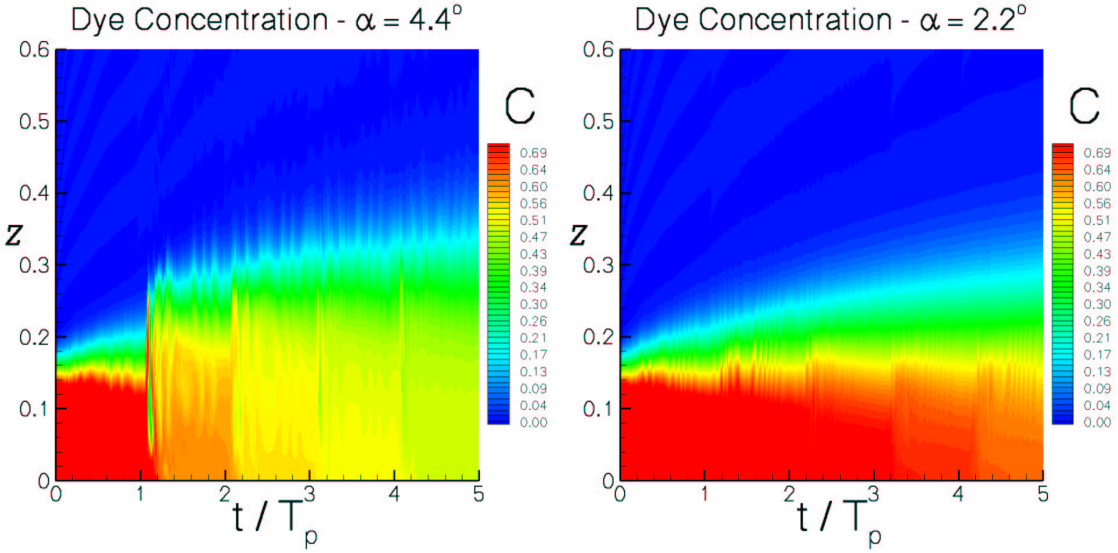

Figure 8. Horizontally averaged dye concentration as a function of time and distance from the boundary for two different experiments.

It is apparent that the combination of tidal ellipses, the bottom Ekman layer, stratification, and buoyant intrusions can produce efficient pathways for the new intermediate density water formed in the mixing phase to leave the boundary layer. The boundary layer is observed to become strongly restratified between mixing cycles. The time progression of the mixing of scalar tracer dye as a function of time is shown in Figure 8 for two cases over different bottom slopes. In both cases there is a steady thickening of the dye layer. The initial conditions are $C = 1$ for $z < 0.1$ decreasing linearly to $C = 0$ at $z = 0.2$. The turbulent layer for $\alpha = 4.4^o$ is significantly thicker (*cf.* Figure 6) than for $\alpha = 2.2^o$ and the vertical spreading of the dye across the active mixing region occurs more rapidly.

The amount of tidal potential energy that is released to turbulent mixing in the benthic boundary layer on the slope is directly related to the boundary layer thickness, or more precisely to the momentum thickness, θ, defined as $\theta(t) = \int_0^{\delta} \frac{u}{U_\infty}\left(1 - \frac{u}{U_\infty}\right) dz$.

Here, *u(z)* is the horizontally averaged instantaneous upslope velocity profile and δ is the boundary layer thickness, above which the free stream velocity is within 1% of U_∞. This is depicted pictorially in Figure 9.

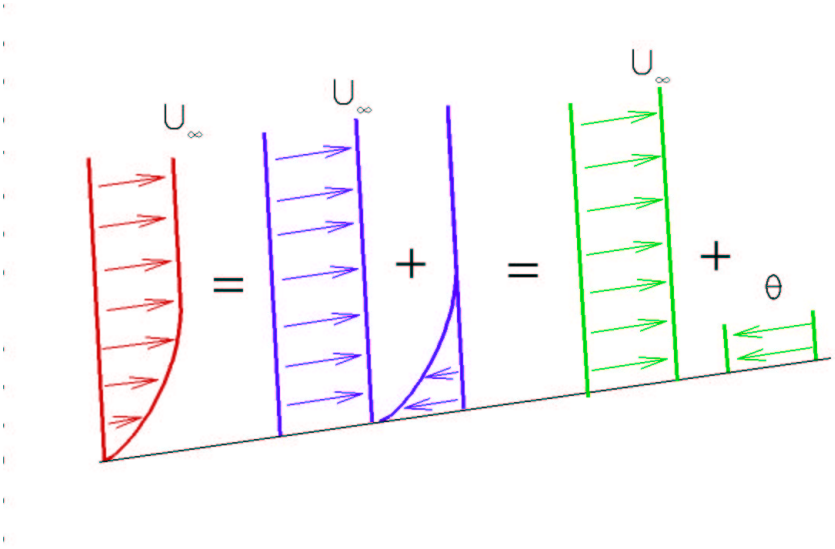

Figure 9. The momentum thickness (green) is the distance, θ, that would have the same net momentum flux as the depth integrated velocity deficit (blue) of the boundary layer (red) if it were moving at the free stream velocity U_∞.

For a steady turbulent boundary layer in an unstratified environment, over a flat plate, it is common that the momentum thickness is approximately 10% of the boundary layer thickness. A laminar boundary layer has $\theta \cong 0.15\,\delta$. It is unclear what the relationship between θ and δ in the unsteady flow over a rough wall in the benthic boundary layer in a stratified fluid. Measurements from the simulations were typically between 7 and 20% of δ depending on the phase of the tide.

The flux of available potential energy produced by the process of heavier upslope fluid moving faster on the slope than lighter boundary layer fluid is

$$\frac{dPE_A}{dt} = \int_V \rho g w dV = A_{xy} g \int_0^{\theta} \frac{\partial \overline{\rho}}{\partial z} z U_{\infty}(t) \sin(\alpha) dz = A_{xy} g \frac{\theta^2}{2} U_{\infty} \frac{\partial \overline{\rho}}{\partial z}(t) \sin(\alpha) \qquad (6)$$

where potential energy is defined (Winters et al, 1995) as $PE = g\int_V \rho z dV$.

From this we could estimate the total mixing produced by this process in the deep ocean over a planform area (A_{xy}) as

$$Mixing \approx R_f \beta A_{xy} g \frac{\theta^2}{2} \frac{U_M}{3} \frac{\partial \overline{\rho}}{\partial z} \alpha \qquad (7)$$

where β is the factor accounting for the angle between the principle axis of the barotropic tide and the upslope direction, the small angle approximation is used for $sin(\alpha)$, and the factor $U_M / 3$ accounts for the portion of the wave period when the tide is going upslope and that the average value of U_∞ is less than the maximum velocity U_M. The greatest variability in the formula will be caused by the value of θ, which we estimate to be in the range of 4 - 40 m for different situations, and may be strongly dependent on the bottom roughness, and on $\frac{\partial \overline{\rho}}{\partial z}$ which changes by approximately 2 orders of magnitude across the ocean depth. Taking some ballpark numbers for these quantities, given the large value of A_{xy}, it is simple for the reader to show that the release of tidal potential energy by this process could produce in the range of 0.1 – 1 TW of mixing in the ocean (cf. Munk and Wunsch, 1998). Improved areal estimates, utilizing methods of Egbert and Ray (2001) are a focus of our ongoing work.

4. Summary

In preliminary analyses of HOME data, Boyd et al. (2002) observed that there are significant density overturns near the slope boundary on an oceanic ridge and that these events are correlated with tidal phase and modulation. We utilize numerical simulations to examine the dynamics of an idealized barotropic tide in a stratified fluid on a slope with environmental parameters similar to HOME conditions. Consistent with the observations, model predictions show that mixing is enhanced during the phase when the tide is approaching its maximum upslope excursion and begins to return down slope. We find that the frictional boundary layer can produce significant release of tidal potential energy to turbulent mixing as heavier water moves upslope and overtakes lighter fluid trapped in the boundary layer. The convective mixing persists for a 0.2 to 0.4 T depending on the slope and the stratification. During phases when the tide is moving downslope, the process arrests and the boundary layer becomes strongly stratified, as the opposite process dominates, as lighter water moves downslope but heavier fluid is trapped in the boundary layer. The strong stratification during this phase shuts down mixing in the benthic boundary layer.

Simulations indicate that strong mixing can be produced as the result of complex interactions of buoyancy forces, frictional forces, non-linearity, Coriolis forces, and barotropic pressure gradients. The full oceanic problem is much more rich and complex, including baroclinic modes, critical reflection of internal waves, turbulent Ekman layers, straining of the background density field, and large-scale topographic variability. Our focus has been on the conversion of tidal potential energy to diapycnal mixing of the deep ocean stratification.

5. References

Allen, J. S. and P. A. Newberger, 1998, On symmetric instabilities in oceanic bottom boundary layers, Journal of Physical Oceanography, 28, 1131-1151.

Armi, L., 1978, Some evidence for boundary mixing in the deep ocean, *Journal of Geophysical Research*, 83, 1971-1979.

Blennerhassett, P. J. and A. P. Bassom, 2002, The linear stability of flat Stokes layers, *Journal of Fluid Mechanics*, 464, 393-410.

Boyd, T., M.D. Levine, S.R. Gard, and W. Waldorf, 2002, Mooring Observations from the Hawaiian Ridge, Data Report 185, Ref. #2002-1, Oregon State University, Corvallis, Oregon.

Chant, R. J. and A. W. Stoner, 2001, Particle trapping in a stratified flood-dominated estuary, *Journal of Marine Research*, 59, 29-51.

Egbert, G.D. and R.D. Ray, 2001, Estimates of M2 tidal energy dissipation from TOPEX/Poseidon altimeter data, J. Geophys. Res., 106, 22475-22502.

Eriksen, C. C., 1985, Implications of ocean bottom reflection for internal wave spectra and mixing, *Journal of Physical Oceanography*, 15, 1145-1156.

Gad-El-Hak, M., S. H. Davis, J. T. McMurray, and S. A. Orszag, 1984, On the stability of the decelerating laminar boundary layer, Journal of Fluid Mechanics, 138, 297-323.

Garrett, C., 1991, Marginal mixing theories, *Atmosphere-Ocean*, 29, 313-339.

Holloway P.E. and M. A. Merrifield, 1999, Internal tide generation by seamounts, ridges, and islands, *Journal of Geophysical Research*, 104 (C11), 25937-25951.

MacCready, P., Rhines, P. B., 1991, Buoyant inhibition of Ekman transport on a slope and its effect on stratified spin up, *Journal of Fluid Mechanics*, 223, 631-661.

Mellor, G. L., and T. Yamada, 1982, Development of a turbulent closure model for geophysical fluid problems, *Reviews of Geophysics*, 20, 851-875.

Merrifield M. A., Holloway P. E., Johnston, T. M.S., 2001, The generation of internal tides at the Hawaiian Ridge, *Geophysical Research Letters*, 28 (4), 559-562.

Munk, W, and C. Wunsch: 1998: Abyssal recipes II: Energetics of tidal and wind mixing, *Deep-Sea Research*, 45, 1977-2010.

Phillips, O. M., 1970, On flows induced by diffusion in a stably stratified fluid, *Deep-Sea Research*, 17, 435-443.

Simpson, J. H., J. Brown, J. Matthews, and G. Allen, 1990, Tidal straining, density currents and stirring in the control of estuarine stratification, *Estuaries*, 13, 125-132.

Slinn, D. N. and J. J. Riley, 1998b, Turbulent dynamics of a critically reflecting internal gravity wave, *Theoretical and Computational Fluid Dynamics*, 11, 281-303.

Slinn, D. N. and J. J. Riley, 1998a, A model for the simulation of turbulent boundary layers in an incompressible stratified flow, *Journal of Computational Physics*, 144, 550-602.

Slinn, D. N. and J. J. Riley, 1996, Turbulent mixing in the oceanic boundary layer caused by internal wave reflection from sloping terrain, *Dynamics of Atmospheres and Oceans*, 24, 51-62.

St. Laurent, L. and C. Garrett, 2002, The role of internal tides in mixing the deep ocean, *Journal of Physical Oceanography*, 32, 2882-2899.

Stokes, G. G., 1845, On the theories of the internal friction of fluids in motion, *Transactions Cambridge Philosophical Society*, 8, 287.

Van Aken, H. M., 1986, Onset of seasonal stratification in shelf seas due to differential advection, *Continental Shelf Research*, 5, 475-485.

Winters, K. B., P. N. Lombard, J. J. Riley, E. A.D'Asaro, 1995, Available potential energy and mixing in density-stratified fluids, *Journal of Fluid Mechanics*, 289, 115-128.

Wunsch, C., 1970, On oceanic boundary mixing, *Deep-Sea Research*, 17, 293-301.

Zikanov, O., D. N. Slinn, 2001. Along-slope current generation by obliquely incident internal waves, *Journal of Fluid Mechanics*, 445, 235-261.